

Geochemistry, Geophysics, Geosystems

RESEARCH ARTICLE

10.1029/2024GC011570

Key Points:

- Dense seismic array provides detailed resolution of the crustal thickness and Moho geometry beneath the Appalachians of NW Massachusetts
- Crustal thickness beneath Laurentia
 (~44 km) and accreted terranes
 (~32 km) is very different with a
 complex transition zone and a possible
 step-like Moho geometry
- An anisotropic layer near the zone of Moho complexity indicates a highly deformed zone near the base of the

Supporting Information:

Supporting Information may be found in the online version of this article.

Correspondence to:

R. Masis, rjm449@eps.rutgers.edu

Citation:

Masis, R., Long, M. D., Karabinos, P., & Bourke, J. (2024). Lithospheric structure in the northern Appalachian Mountains: A detailed examination of the abrupt change in crustal thickness in northwestern Massachusetts. *Geochemistry*, *Geophysics*, *Geosystems*, 25, e2024GC011570. https://doi.org/10.1029/2024GC011570

Received 19 MAR 2024 Accepted 7 AUG 2024

© 2024 The Author(s). Geochemistry, Geophysics, Geosystems published by Wiley Periodicals LLC on behalf of American Geophysical Union.

This is an open access article under the terms of the Creative Commons

Attribution License, which permits use, distribution and reproduction in any medium, provided the original work is properly cited.

Lithospheric Structure in the Northern Appalachian Mountains: A Detailed Examination of the Abrupt Change in Crustal Thickness in Northwestern Massachusetts

Roberto Masis¹, Maureen D. Long², Paul Karabinos³, and James Bourke¹

¹Department of Earth and Planetary Sciences, Rutgers University, Piscataway, NJ, USA, ²Department of Earth and Planetary Sciences, Yale University, New Haven, CT, USA, ³Department of Geosciences, Williams College, Williamstown, MA, USA

Abstract Previous geophysical studies in the New England Appalachians identified a ~15 km offset in crustal thickness near the surface boundary between Laurentia and the accreted terranes. Here, we investigate crustal structure using data from a denser array: New England Seismic Transects experiment, which deployed stations spaced ~10 km apart across the Laurentia-Moretown terrane suture in northwestern Massachusetts. We used receiver function (RF) analysis to detect *P* to *SV* converted waves and identified multiple interfaces beneath the transect. We also implemented a harmonic decomposition analysis to identify features at or near the Moho with dipping and/or anisotropic character. Beneath the Laurentian margin, the Ps converted phase from the Moho arrives almost 5.5 s after the initial *P* wave, whereas beneath the Appalachian terranes, the pulse arrives at 3.5 s, corresponding to ~48 and ~31 km depth, respectively. The character of the RF traces beneath stations in the middle of our array suggests a complex transitional zone with dipping and/or anisotropic boundaries extending at least ~30 km. This extension is measured in our profiles and perpendicular to the suture. We propose one possible crustal geometry model that is consistent with our observations and results from previous studies.

Plain Language Summary We explore the crustal structure that developed during the formation of the Appalachian Mountains beneath northwestern Massachusetts during the Paleozoic. In this region, the geology reflects the accretion of multiple terranes onto Laurentia, the ancient core of North America. Previous studies using seismic data have shown evidence for crustal geometries beneath New England that reflect a complex tectonic history of the formation of the Appalachians. We processed recordings of waves from distant earthquakes measured at seismic stations including the New England Seismic Transects array, which has seismic observatories spaced about 10 km apart. This approach allows a clear visualization of the deep crustal geometry beneath the area. We found evidence for a sharp contrast in crustal thickness near the boundary between Laurentia and the Moretown terrane, which was the first terrane accreted. Near the boundary between these terranes, we found evidence for a complex and overlapping set of crust-mantle interfaces. We also identified a highly deformed crust with a layer that shows strong seismic anisotropy (the directional dependence of seismic wave speeds). We created a model for the evolution of crustal structure based on the interpretation of our seismic results along with previous studies based on thermochronologic, paleogeographic, and geophysical data.

1. Introduction

The New England Appalachians are composed of several terranes derived from Gondwana that were successively accreted by distinct orogenic processes during the Paleozoic (Figure 1a). The suture between Laurentia and the Gondwanan-derived terranes occurs at the western margin of the Moretown terrane, the first terrane accreted onto Laurentia during the formation of the Appalachians. This suture has been well-mapped in western New England and marks a critical geologic and geophysical boundary between the Laurentian and Appalachian lithospheres. In contrast, the boundaries between the accreted terranes themselves (including the Moretown and other Gondwanan-derived terranes Ganderia and Avalonia; Figure 1a) are more difficult to distinguish in New England due to their similar geologic characteristics, burial by post-accretion sediments, poor exposure, lack of a clear geophysical signature, and overprinting by post-accretion deformation (Hatcher, 2010; Karabinos et al., 2017; Luo et al., 2022; Macdonald et al., 2014; Waldron et al., 2022). Despite these challenges, understanding the

MASIS ET AL. 1 of 20

15252027, 2024, 10, Downloaded from https://agupubs.onlinelibrary.wiley.com/doi/10.1029/2024GC011570 by Yale University, Wiley Online Library on [23/10/2024]. See the Terms and Condition

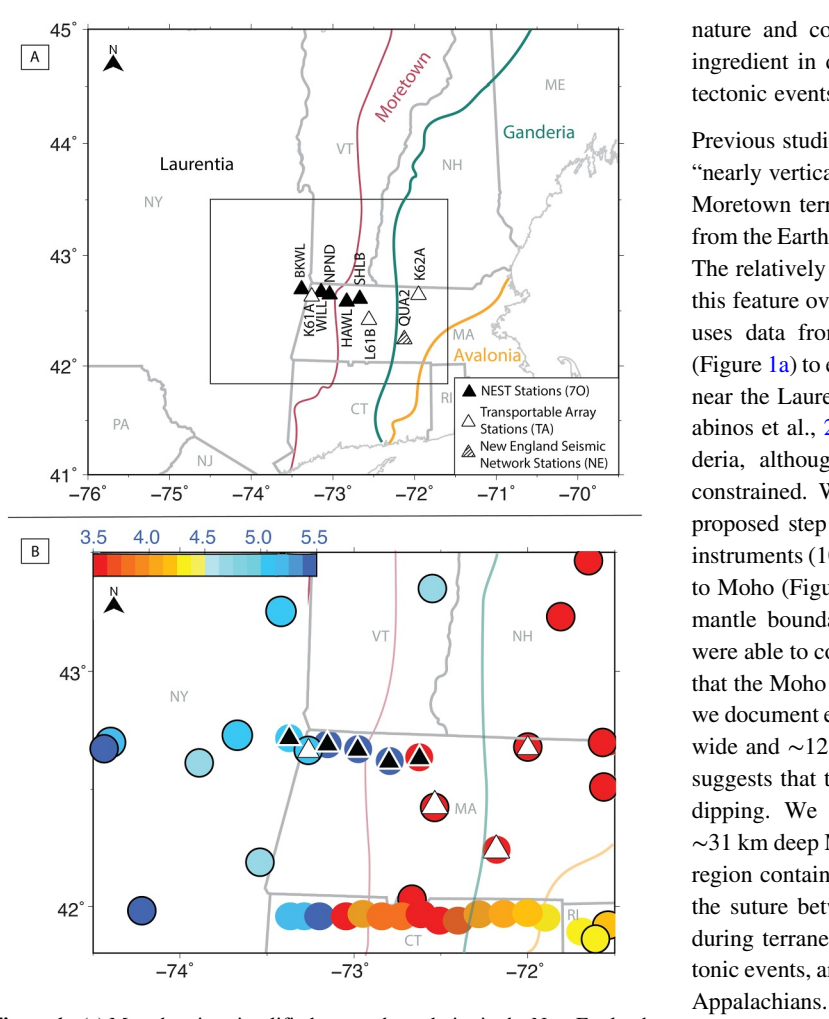


Figure 1. (a) Map showing simplified terrane boundaries in the New England Appalachians. Note that the boundary between Ganderia and the Moretown terrane is not exposed at the surface. Rectangle shows area enlarged in (b). Abbreviations indicate state names (ME, Maine; NH, New Hampshire; VT, Vermont; RI, Rhode Island; CT, Connecticut; NY, New York; NJ, New Jersey; PA, Pennsylvania). (a) Seismic station array used in this study. Solid triangles are New England Seismic Transects stations, open triangles are stations of the Transportable Array (TA), and shaded triangles are stations of the New England Seismic Network (NE). (b) Ps delay times presented in C. Li et al. (2018) (black border circles), Luo et al. (2021) (clear border circles) and this study (triangles). Tectonic terrane boundaries modified from Karabinos et al. (2017). Note that the boundary between the Moretown terrane and Ganderia is approximate.

nature and configuration at the depth of terrane boundaries is a crucial ingredient in deciphering the tectonic history of the Appalachians and the tectonic events that shaped them.

Previous studies were able to identify a ~15 km Moho offset described as a "nearly vertical or steep eastward dipping boundary" between Laurentia and Moretown terrane in southern New England (C. Li et al., 2018) using data from the EarthScope Transportable Array, with stations spaced ~70 km apart. The relatively coarse resolution of this array only allowed them to constrain this feature over a roughly 50 km horizontal distance (Figure 1b). Our study uses data from a dense seismic transect in northwestern Massachusetts (Figure 1a) to explore the finer details of crustal structure and Moho geometry near the Laurentian-Moretown suture. Our transect crosses the suture (Karabinos et al., 2017; Macdonald et al., 2014) and may extend east into Ganderia, although the eastern margin of the Moretown terrane is poorly constrained. We carried out a detailed seismological investigation of the proposed step in crustal thickness with an array of closely spaced seismic instruments (10-15 km) to improve the lateral resolution of the offset in depth to Moho (Figure 1a). We confirmed the abrupt 15 km decrease in the crustmantle boundary depth from Laurentia to the Moretown terrane, and we were able to constrain its location more precisely. However, our data suggest that the Moho offset is not a simple step-like near-vertical structure. Instead, we document evidence for a complex zone of overlap, approximately ~30 km wide and ~12 km deep, coincident with the Moho offset. Seismic evidence suggests that the zone of overlap is anisotropic and that structures are eastdipping. We suggest that in the zone of overlap there is a shallower ~31 km deep Moho above a deeper ~48 km-deep Moho, and that the overlap region contains both mantle and crustal rocks. These complex features near the suture between Laurentia and the Moretown terrane may have formed during terrane accretion or during post-accretion modification by later tectonic events, and are critical to our understanding of the tectonic history of the

More generally, a better understanding of the present-day upper lithospheric structures of the Appalachians is important to unravel the tectonic history of this complex orogen. A detailed picture of the crustal geometry of the suture zone between Laurentia and the Gondwanan-derived Moretown terrane is necessary to understand the attempted subduction of the Laurentian margin, the accretion of the Moretown terrane, and post-accretion deformation of the suture. The steep gradient in depth to Moho identified between the Laurentian margin and the westernmost Gondwanan-derived terrane in southern New England (C. Li et al., 2018; Luo et al., 2021, 2022; this study) is not typical of other segments in the northern, central, and southern Appalachians (Hopper et al., 2016; C. Li et al., 2020; Long & Aragon, 2020; Luo et al., 2023), and appears to record post-Taconic modification of the suture. The detailed geometry of the Moho offset is critical for our understanding of terrane accretion

and can be used to test competing tectonic models. Specifically, if the Moho offset is a nearly vertical suture between Laurentia and the Moretown terrane, it suggests that Gondwanan-derived terranes in the New England Appalachians may be on top of their original intact mantle lithosphere (e.g., C. Li et al., 2018). In contrast, a more complex transition, such as that suggested by our data, implies that the Laurentian lithosphere extends beneath the Moretown terrane, and this interpretation allows the possibility that the accreted terranes were separated from their original mantle lithosphere during Paleozoic orogenesis.

governed by the applicable Creative Commons License

2. Background

2.1. Tectonic History

The Neoproterozoic breakup of the supercontinent Rodinia created a rifted margin parallel to the Mesoproterozoic Grenville orogen (e.g., Hatcher, 2010). The Appalachians developed along this margin during several Paleozoic orogenic events. The first event, the Taconic orogeny, occurred when the Moretown terrane collided with the Laurentian margin above an east-dipping subduction zone during the Early to Middle Ordovician (Karabinos et al., 2017; Macdonald et al., 2014). During the Taconic orogeny, a reversal in subduction polarity resulted in west-dipping subduction under the modified Laurentian margin (Karabinos et al., 2017; Macdonald et al., 2014). However, other researchers have proposed that the entire Taconic orogeny developed during collision above an east-dipping subduction zone (Hildebrand & Whalen, 2020; Valley et al., 2019). Late Ordovician to Early Silurian Salinic orogeny occurred when Ganderia was accreted to the Laurentian margin (van Staal et al., 2009). Accretion of the Avalon terrane during the Late Silurian to Devonian Acadian orogeny overprinted much of New England and obscured the record of the Salinic and Taconic orogenies (Bradley et al., 2000). The Late Devonian to Mississippian Neoacadian orogeny has been attributed to the accretion of Meguma (van Staal et al., 2009), which is not recognized as a separate terrane in New England. The culminating orogeny in the development of the Appalachians was the Pennsylvanian to Permian Alleghenian orogeny, in which Gondwana collided with Laurentia to form the supercontinent Pangea (Hatcher, 2010).

2.2. Previous Studies: Geology

Macdonald et al. (2014) and Karabinos et al. (2017) proposed that the Moretown terrane is the westernmost Gondwanan-derived terrane, based on detrital zircon data that show that the meta-sedimentary Moretown Formation was sourced from Gondwanan crust. They suggested that the Shelburne Falls arc formed on the Moretown terrane as it approached Laurentia above an east-dipping subduction zone. Following collision in the Early Ordovician, subduction polarity reversed and a west-dipping subduction zone developed outboard of the Moretown terrane. This study further supports the idea that the suture between Laurentia and the Moretown terrane may be a lithospheric-penetrating east-dipping structure. We also explore the hypothesis that the transition from the Grenville margin to the accreted terranes can be identified at depth using geophysical data, particularly the western boundary of the Moretown terrane, which represents the beginning of the accretion processes of Gondwanan-derived terranes.

Hillenbrand et al. (2021) presented petrologic and ⁴⁰Ar/³⁹Ar thermochronological data that argued for the existence of an Acadian plateau in southern New England from 380 to 330 Ma, with crustal thickness exceeding 60 km following peak metamorphic conditions. This suggests that the crust in this region was significantly thinned during the Acadian Orogeny, which has important implications for interpretations of the current geometry of the crust. The western border of the hypothesized plateau closely coincided with the suture between Laurentia and the Moretown terrane, as well as the 15 km offset in the depth to Moho identified by C. Li et al. (2018). Hillenbrand et al. (2021) proposed that the formation and collapse of the so-called Acadian Altiplano may have played a major role in forming the Moho offset documented by C. Li et al. (2018).

2.3. Previous Geophysical Imaging

Previous geophysical imaging of the crust beneath New England has encompassed both active-source (reflection and/or refraction) profiling and passive source deployments. Crustal-scale refraction/reflection profiling by Hughes and Luetgert (1991) along three roughly east-west lines to the north of the New England Seismic Transects (NEST) deployment identified clear differences in crustal *P* wave velocities between the Laurentian Grenville crust and the Appalachian terranes to the east. These authors described an eastward-dipping ramp-like structure in the mid-crust and identified evidence for a particularly fast lower Grenville crust. However, they did not find evidence for a significant difference in thickness between the Grenville and Appalachian crusts. Results from COCORP reflection profiling in New York, Vermont, and New Hampshire (Ando et al., 1984; Brown et al., 1983) also found evidence for ramp-like structures in the mid-crust connecting Grenville basement with accreted Appalachian terranes; however, their profiles did not shed any light on crustal thickness or its lateral variability.



Wiley Online Library on [23/10/2024]. See

Taking advantage of the relatively dense (\sim 70 km station spacing) network of broadband stations deployed as part of the EarthScope USArray Transportable Array effort, C. Li et al. (2018) used receiver function (RF) analysis to characterize crustal thickness beneath \sim 200 stations in the northeastern U.S. and southeastern Canada. They focused on the arrival times of *P*-to-*S* converted waves from the Moho and found a variation in the range of 3–6 s after the *P* wave arrival (Figure 1b), which they interpreted as corresponding to Moho depths between 27 and 52 km. They concluded that the crustal thickness decreases from the Grenville belt eastward toward the Atlantic coast, which is supported by other studies (Savage et al., 2017; Schmandt et al., 2015; Shen & Ritzwoller, 2016). C. Li et al. (2018) further noted that while a decrease in crustal thickness from Grenville to Appalachian terranes is a general feature of the northern Appalachians, there are some regions where this lateral transition appears to be particularly sharp. They suggested that beneath southern New England, this transition takes on a "step-like" character, with a difference in crustal thickness from around 45 km in the west to around 30 km depth in the east accommodated over an E-W horizontal distance of \sim 50 km. The work of C. Li et al. (2018) established the relevance of this feature has for understanding the tectonic history of the New England Appalachians. Crucially, their results also argue for the acquisition of additional seismic data to facilitate the detailed imaging of this crustal transition with higher spatial resolution.

Luo et al. (2021) analyzed data from a dense seismic array (SEISConn) consisting of 15 broadband stations located to the south of our study area in northern Connecticut, also using P-to-S converted waves, and Luo et al. (2022) used scattered wave imaging targeting the Moho. Both studies identified an abrupt change in depth to Moho; the western part of the array shows a deeper Moho boundary (\sim 45 km) than the central and eastern sides of the array (\sim 30 km). This abrupt decrease in depth to Moho of \sim 15 km occurs over a \sim 20 km horizontal distance (Figure 1b). Luo et al. (2021, 2022) discussed three possible models for the formation of the abrupt change in depth to Moho: the step might have resulted from (a) the juxtaposition of crustal blocks during the Taconic orogeny with preexisting differences in thickness, (b) under-thrusting of Laurentia beneath the Moretown terrane during the Taconic orogeny, or (c) overprinting by younger tectonic events (Acadian/Neoacadian) that steepened a more gradual transition in crustal thickness.

2.4. Goals of This Study

Motivated by these previous results, we focus on the nature of the transition from the Grenville belt of Laurentia to the accreted Appalachian crust at a latitude of 42.6°N in western Massachusetts and eastern New York (Figure 1). The dense NEST array line is located roughly 75 km north of the dense SEISConn line, allowing us to examine whether the Moho geometry imaged beneath SEISConn (Luo et al., 2021, 2022) extends to the north, thereby shedding light on potential along-strike variability in the northern Appalachians. The dense NEST line also allows us to probe the transition between thick Grenville crust and thinner Appalachian crust beneath western Massachusetts in much greater detail than was possible using USArray data alone (C. Li et al., 2018). Specifically, the seismic stations on either side of the proposed Moho offset (C. Li et al., 2018) are K61A and L61B; both are included in our study, but we also use data from an additional five stations of the NEST array that allow for substantially better lateral resolution. More precise constraints on the geometry of the Moho beneath western Massachusetts will allow for more specific testing to support or refute previously formulated hypotheses to explain the crustal structure below New England. These include the Acadian plateau hypothesis of Hillenbrand et al. (2021, 2022), which invokes a role for plateau formation and collapse in shaping the architecture of the Moho beneath southern New England, the cumulative effects of Paleozoic accretion and crustal shortening events suggested by C. Li et al. (2018), and the vertical displacement due to Acadian crustal shortening proposed by Luo et al. (2022). Our research represents the first detailed (~10 km station spacing) broadband seismic imaging targeting the crustal structure beneath western Massachusetts, helping to establish how the crustal architecture varies along strike within New England and within the Appalachian Orogen more broadly.

3. Methodology

3.1. RF Analysis

We used RF analysis (e.g., Ammon, 1991; Langston, 1979) to detect *P* to *S* converted waves associated with boundaries in the crust and mantle. This method assumes that *P*-to-*S* conversions take place at boundaries where abrupt changes in impedance (velocity times density), including those associated with seismic anisotropy, take place. The polarities and amplitudes of the phases resulting from these conversions reflect the nature of the



Table 1
Data Statistics and Results for Each Station

Station	Network	Crustal thickness (km)	Ps delay times (s)	Latitude/Lon	Start date	End date	Total of events used
BKWL	70	42	4.8	42.724/-73.366	2019-08-04	2020-08-18	18
K61A	TA	45	5.1	42.669/-73.267	2013-10-12	2015-09-24	65
WILL	70	46	5.2	42.712/-73.206	2018-10-22	2021-08-11	82
NPND	70	46	5.2	42.652/-73.051	2019-06-24	2021-07-29	8
HAWL	70	46	5.2	42.610/-72.912	2018-10-22	2021-06-06	57
SHLB	70	31	3.5	42.601/-72.750	2019-07-31	2021-08-14	45
L61B	TA, N4	31	3.5	42.449/-72.680	2013-09-14	2019-03-01	272
QUA2	NE	29	3.3	42.280/-72.350	2010-06-12	2018-05-04	266
K62A	TA, N4	30	3.4	42.665/-72.234	2013-09-15	2019-02-17	233

changes in properties across the boundaries. In the case of *P*-to-*SV* conversion at a horizontal interface, a positive polarity implies that the impedance increases with depth across the boundary, and vice versa for negative polarities. A combination of impedance contrast, anisotropy, and boundary dip determines the polarity and amplitude of *P*-to-*SH* converted waves (Levin & Park, 1998).

We worked with data from five stations, spaced roughly 10 km apart, from the dense NEST (Long & Levin, 2018) experiment (network 70). These stations (BKWL, WILL, NPND, HAWL, and SHLB) were located in eastern New York or northwestern Massachusetts (Figure 1b). The NEST array was intended to fill the station gap that C. Li et al. (2018) encountered directly above the putative Moho "step" and therefore to obtain more detailed resolution. We also included data from long-operating sites that belonged to the EarthScope Transportable Array Network (TA) (IRIS Transportable Array, 2003): K61A, K62A, and L61B, and the New England Seismic Network (NE): QUA2, which have been included in previous research on the step. Data for sites K62A, QUA2, and L61B were assembled by Y. Li et al. (2021); we reprocessed these data in our study. We thus include results from nine seismic stations in total. Table 1 shows the date range of data used at each station and the number of events used per station to carry out the RF analysis.

We selected earthquakes with minimum magnitudes of 5.5 at epicentral distances between 20° and 180° , a distance range that has been successfully used in previous similar studies (Bourke et al., 2020; Levin et al., 2023). We used P, $P_{\rm diff}$, and PKP phases (Storchak et al., 2008) in our analysis. We applied a quality control procedure, relying on visual inspection, to eliminate traces with obvious phase interference, including triplicated waves. A total of 1,046 teleseismic earthquakes were used; of these, 210 occurred during the time period of NEST array deployment beginning in Fall 2018 (we used data through Summer 2021). We collected three-component records of P waves from teleseismic events and performed a visual inspection of their quality. Prior to RF analysis, we rotated the three-component seismograms to a coordinate system aligned with the incoming P wave ray (LQT). We expect the resulting waveforms to represent compressional waves on the L component, which is meant to be aligned with the incoming P wave ray, converted P-SV phases on the Q component, as a result of impedance contrasts between layers at depth, and converted P-SV phases on the T component with directionally dependent amplitudes and polarities (e.g., Chen et al., 2021; Y. Li et al., 2021).

The Multitaper Spectral Correlation (MTC) algorithm is advantageous for the computation of RFs for waveforms with significant levels of noise (Park & Levin, 2000). RF traces derived from multiple earthquake records at a single station can be combined via stacking into a single RF time series; such stacks are typically binned by either backazimuth or epicentral distance. Before processing individual records into backazimuth or epicentral bins, we corrected all seismograms for the incidence angle of the *P* wave. This correction relies on the value of the incidence angle for incoming *P* waves as predicted using a 1D global velocity model such as IASP91 (Kennett & Engdahl, 1991). We adjusted the velocity models used to perform the correction (e.g., Park & Levin, 2016) using site-specific values of seismic velocities from Y. Li et al. (2021).

The time delay of the P-to-S converted wave relative to its parent P wave is proportional to the depth of the converting boundary (e.g., Gurrola & Minster, 1998), according to:



where t is the delay of the converted phase, V_p and V_s are the velocities of the P and S waves, and p is the ray parameter. In our analysis, the ray parameter is zero since we corrected all data to approximate vertical incidence.

Infinitely sharp boundaries will cause conversions at all frequencies, while a diffuse boundary will only cause conversions for relatively long wavelengths. Levin et al. (2016) showed that the maximum vertical distance D over which the properties change is related to the wavelength λ of the converted P-SV wave, as given by:

$$D = \frac{\lambda}{4} \frac{\frac{V_P}{V_S}}{\frac{V_F}{V_S} - 1}.\tag{2}$$

We therefore processed our data using a range of maximum frequency values (0.25–1 Hz) to compare the response of the features at each frequency and thus infer the sharpness of the velocity change at each boundary. At higher frequencies (shorter wavelengths), Ps converted waves will not be generated if the change in impedance is accommodated over a broad depth range. However, a downside of the higher-frequency data is generally higher noise levels. Lower frequencies, by contrast, may yield RF traces with higher signal-to-noise ratio and thus more robust results; however, they obscure detailed structure that may be visible at higher frequencies.

We also applied the harmonic decomposition technique, which can help us to understand the nature of complexity at the converting boundary by targeting variations of RF traces as a function of direction (as expressed by the backazimuth). A horizontal, isotropic boundary in impedance is expected to produce identical *P-SV* converted waves from all directions, and no *P-SH* waves. A boundary in anisotropic seismic velocity leads to directionally variable amplitudes and polarities of *P-*to-*S* converted waves (e.g., Bostock, 1998; Levin & Park, 1997). Similarly, a dipping isotropic boundary will also lead to directional variability. A number of previous studies have explored how dipping and/or anisotropic boundaries express themselves in RF data and have applied harmonic decomposition analysis or similar techniques to characterize boundaries using real data (e.g., Bianchi et al., 2010; Levin & Park, 1997; Olugboji & Park, 2016; Schulte-Pelkum & Mahan, 2014). Expected variations for (laterally homogenous) anisotropic models have patterns with periodicities of 180° (i.e., with an amplitude proportional to a sum of sin(baz) and cos(baz) terms) and/or 90° (i.e., with an amplitude proportional to a sum of sin(2*baz) and cos(2*baz) terms), where "baz" is the backazimuth, with the relative proportion of the terms depending on the orientation of the symmetry axis. A 180° periodic pattern is expected for a dipping (isotropic) impedance boundary.

We applied the harmonic decomposition method (Park & Levin, 2016) for RF modeling to the Q and T components of our RF data simultaneously, and used the results to identify the dipping and/or anisotropic character of the interfaces. The relative contributions of RF timeseries components are evaluated by fitting a scaled sum of five harmonic functions (constant, cos(baz) and sin(baz), cos(2baz) and sin(2baz)). Energy registered on the cos(baz) or sin(baz) terms implies that the corresponding boundary is dipping and/or that anisotropy is present with a plunging axis of symmetry. Energy on the cos(2*baz) or sin(2*baz) terms implies a contrast in anisotropy in the horizontal plane (i.e., azimuthal anisotropy). We perform the harmonic decomposition following the procedures described in detail in Chen et al. (2021) and Y. Li et al. (2021). One challenge with this method is the differentiation between a dipping interface and anisotropy with a plunging symmetry axis. Furthermore, harmonic decomposition rests on the assumption that the structure at depth is laterally homogeneous and is being sampled across all directions. When this assumption is violated, as in the case of lateral heterogeneity or strongly dipping interfaces, the pulses on the harmonic terms will be more complex to interpret. Also, when using anisotropyaware RF analysis, including the harmonic decomposition method, it is often ambiguous as to whether the anisotropy lies above or beneath an anisotropic interface. In this study, we have identified possible depth ranges of anisotropic layers based on the inferred depth of the interfaces indicated by RF analysis. We have taken these methodological limitations into consideration during the interpretation stage of this study.



3.2. Interpretation of Boundary Depths

We estimated the depths of the boundaries identified in our analysis assuming a ratio of compressional and shear wave speeds (V_p/V_s) of 1.73. This V_p/V_s value is derived from an average for stations K61A, K62A, QUA2, and L61B taken from the IRIS EARS RF database (Trabant et al., 2012), which estimated bulk crustal V_p/V_s based on an H-k stacking approach (Zhu & Kanamori, 2000). The same crustal compressional wave speed value, $V_p = 6.419$ km/s, was used for all four sites in the EARS database, and we also adopted this value in our modeling. We picked delay time values at the peak of each pulse and used Equation 1 to evaluate the depths of the converting boundaries beneath each site.

We tested the influence of the V_p/V_s ratio on our depth estimates, experimenting with V_p/V_s values of 1.79 for stations in the western part of our array (BKWL, K61A, WILL, NPND, and HAWL) and 1.71 for the stations in the eastern part (SHLB, L61B, QUA2 and K62A). These test values are based on the IRIS EARS RF database (Trabant et al., 2012). When these test values were used, stations in the western part of our array yielded crustal thickness estimates ~4 km smaller and stations in the eastern part of our array yielded estimates ~1 km greater (Tables S1 and S2 in Supporting Information S1). While we do not apply H-k stacking in our study, complementary recent work by Bourke, Link et al. (2023) and Bourke, Vadim et al. (2023) computed H-k stacks for ~150 seismic stations throughout New England, including stations of the NEST array; they noted that the significant complexity in the vicinity of the Moho step made robust estimation of crustal V_p/V_s beneath NEST stations difficult.

4. Results

4.1. Single-Station Analysis Example: Station SHLB

To illustrate our data processing and analysis procedures, we show in Figure 2 results from our RF analysis from the NEST station SHLB. Data from TA station L61B are also shown in this figure for comparison, as discussed further below. SHLB recorded 45 usable P waves suitable for analysis (Figure 2a). We first combined all Q-component RFs into a single trace (Figure 2b), corrected for moveout, that represents an average of the energy recorded on this component across all 45 events. We also show the RF time series for components Q and T as a function of backazimuth, binned in increments of 5° (Figure 2c). Note that earthquake sources with backazimuths between 0° and 100° (coming from the east) are very scarce (Figure 2a), with a single RF signal at \sim 15° (Figure 2c). Data coverage increases for backazimuths between 100° and 360° (Figure 2a), which results in more densely sampled backazimuth bins (Figure 2c). We next apply harmonic decomposition analysis, constructing five timeseries that represent the relative contributions of constant and directionally varying amplitudes at each time step in the RF timeseries (Figure 2d). The polarity of the waveforms on the Q components and the constant component of the harmonic decomposition reflect isotropic impedance changes with depth; positive pulses reflect an increase in impedance with depth, like the one expected to occur at the Moho. The polarities of the T component RFs and the directional harmonic components depend on anisotropy symmetry and the sense of impedance changes (cf., Levin & Park, 1998), and are also influenced by dip of the boundary (e.g., Cassidy, 1992) (Figure 2c).

Figure 2b shows the stacked Q component signal registered by station SHLB; the Moho boundary (green line at $\sim 3.5 \text{ s}$) is associated with an increase in impedance with depth (crust-and creates a positive (blue) pulse. The shallower blue pulse (<3 s) represents intra-crustal structure that is not the target for this particular study. Panel C shows RF data for both Q and T components; the change of impedance registered by a horizontal boundary will be reflected on the Q component and if there is a corresponding pulse on the T component, it indicates that the boundary that the seismic waves went through is dipping, anisotropic, or both. For station SHLB, we observe a positive pulse on the T component registered between 0° to 30° and $270^{\circ}-360^{\circ}$ at $\sim 4 \text{ s}$, which means that there is a dipping boundary or anisotropy that affects the seismic energy coming from this range of directions. These results can be further inspected using harmonic decomposition (panel D). In the case of station SHLB, we can visually identify negative impedance (red pulse) on components $\cos(\text{baz})$ and $\cos(2*\text{baz})$ at the time delay associated with the Moho Ps phase; therefore, the Moho boundary has a dipping and/or anisotropic character. We applied these tools to the data registered by all the stations in our array (stations SHLB and L61A shown in Figure 2; other stations shown in Figures S1–S7 in Supporting Information S1).

Wiley Online Library on [23/10/2024]. See

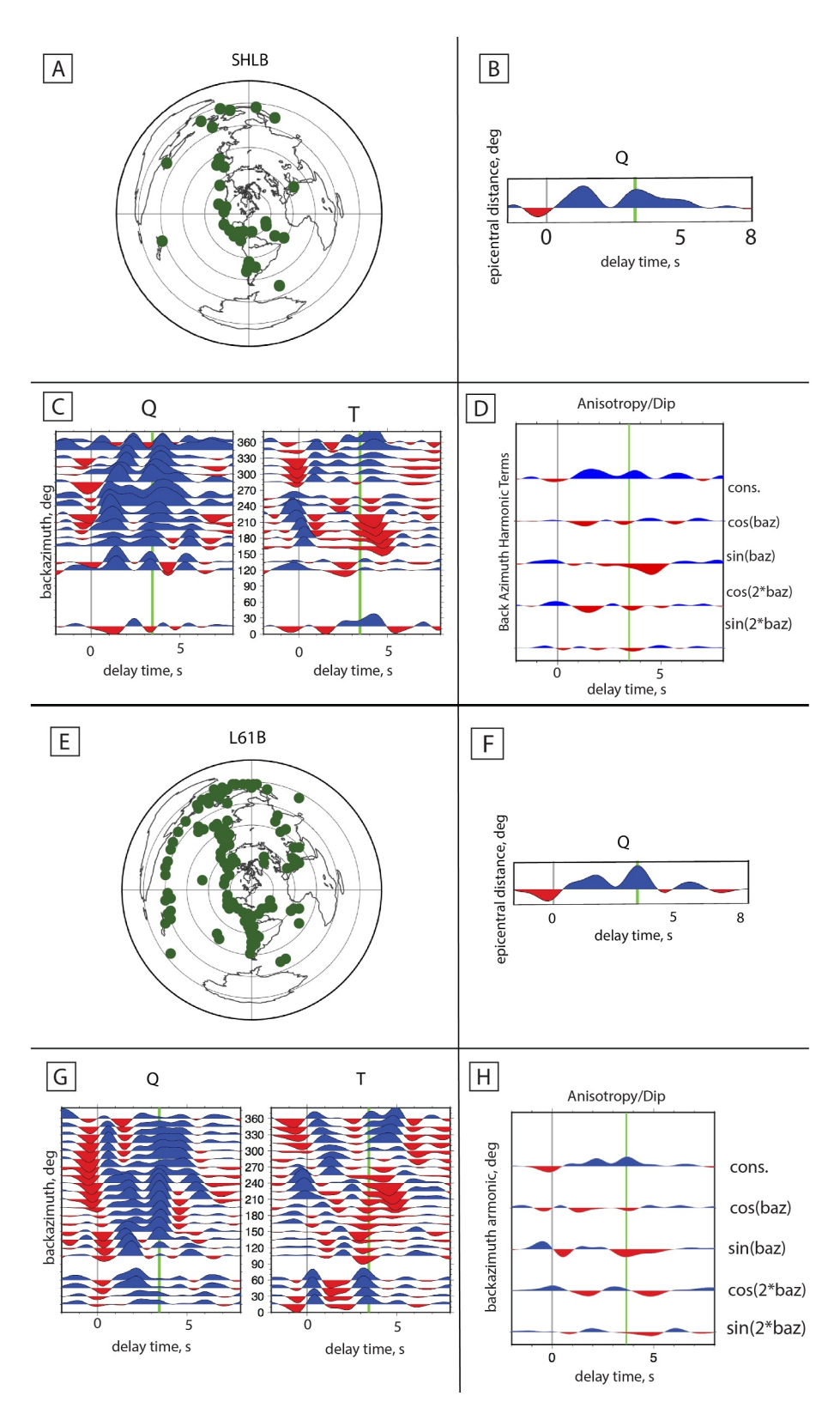


Figure 2.

1523227, 2024, 10, Downloaded from https://agupubs.onlinelibrary.wiley.com/doi/10.10929024GC011570 by Yale University, Wiley Online Library on [23/10/2024]. See the Terms and Conditions (https://onlinelibrary.wiley.com/terms-and-conditions) on Wiley Online Library or rules of use; OA articles are governed by the applicable Centaive Commons Licensea

15252027, 2024, 10, Downloaded from https://agupubs.onlinelibrary.wiley.com/doi/10.1029/2024GC011570 by Yale University, Wiley Online Library on [23/10/2024]. See the Terms

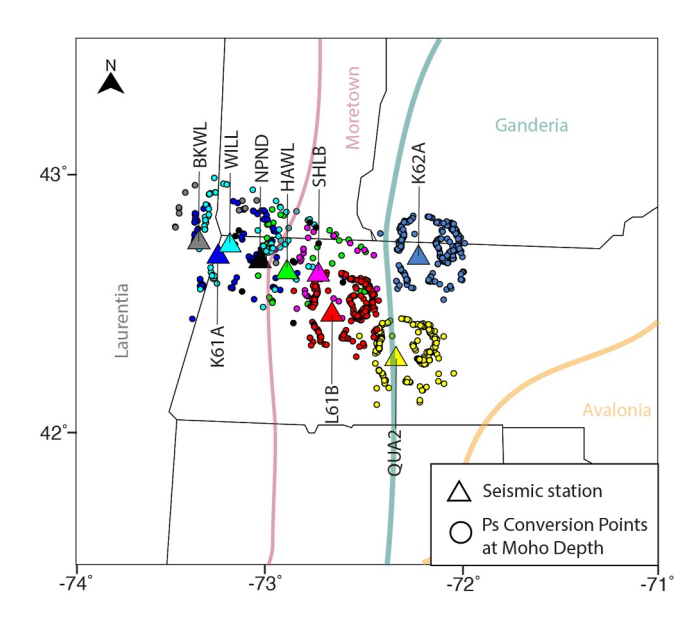


Figure 3. Map showing *P*-to-*S* conversion points at Moho depth around the seismic stations for each earthquake used to compute RFs. The conversion points are color-coded to match the color of the respective seismic stations. The tectonic boundaries between Laurentia and the Gondwanan-derived terranes are represented by colored lines; terranes (Laurentia, Moretown, Ganderia, Avalonia) are labeled. Note that the boundary between the Moretown terrane and Ganderia is approximate; stations QUA 2 and K62A may be on the Moretown terrane.

4.2. Observed RFs Across the NEST Transect

A key result of our study is a transect of single-station stacked receiver functions that represent crustal properties beneath the NEST line (Table 1). To give a sense of how the Ps phases we study are sampling structure at depth, we show in Figure 3 a piercing point diagram for these phases at a depth of 40 km. This diagram demonstrates that the Moho is very well sampled by our data set, but also illustrates the possibility of lateral "smearing" of the structure by our single-station stacking and harmonic decomposition approaches. To rule out the possibility that differences in RFs among different stations represent artifacts of the different amounts of data available at longrunning versus temporary stations, we carried out a down-sampling test using data from long-station QUA2. We compared results from a data set covering 8 years and from a data set that matches the time frame of NEST station operation (~3 years); the results of this test are shown in Figure S8 in Supporting Information S1. While there are some subtle differences, the major features are highly similar, showing that the differences in run times among stations do not affect our conclusions.

Stacked *Q*-component RFs filtered with a maximum frequency of 0.5 Hz and plotted at the location of each of the nine stations we analyzed are shown in Figure 4. Beneath stations at the western end of the array (sites BKWL, K61A, WILL), we identify pulses that correspond to converted Ps phases arriving 5–5.5 s after the initial *P* wave. Sites at the eastern end of the array (QUA2 and K62A) show similar pulses with different timings, closer to 3.5 s. In contrast, sites in the middle of the array (NPND, HAWL, SHLB and L61B) exhibit multiple weak pulses in the 3.5–5.5 s time range that could plausibly

be associated with the Ps arrival, presenting a challenge for interpretation in terms of the crustal thickness, as the pulses might overprint or interfere with each other. Site NPND shows one weak pulse at \sim 5.5 s and a possible pulse at \sim 3 s. These four stations, located in the middle of the array and reflecting a complex geometry at depth, overlie the boundary between Laurentia and the Moretown terrane. We also observed apparent positive pulses at times 0–2 s at most sites and pulses from 3.5 to 5.5 s at sites west of HAWL (Figure 4); these delay times would correspond to the structure in the upper crust at \sim 18 km and between \sim 27 and \sim 43 km, respectively, although the significance of these pulses is uncertain. Because our study is aimed at the Moho geometry, we do not focus our interpretation on these intra-crustal features, although they have been shown to be important in other regions of New England (e.g., Luo et al., 2021).

Our frequency-dependent analysis (Figure 5) shows that the pulses that we have interpreted as Moho boundaries persist at higher frequencies (1 Hz, corresponding to wavelengths of \sim 6.4 km) (Figure 5a). Specifically, we observe a clear pulse at \sim 5 s beneath stations on the west of the array (BKWL, K61A, WILL) and at \sim 3.5 s on the east of the array (QUA2, K62A). These results at high frequency indicate that the boundaries are relatively sharp (\sim 5 km in thickness). For the stations located in the center of our array (NPND, HAWL, SHLB), the pulses at 3.5 and 5 s are not clear and it is difficult to discern the depth of the Moho beneath those stations. For comparison purposes, we include in Figure 5b the seismic energy at 0.5 Hz, which is the same frequency used in Figure 4. Figure 5c shows the results for our data processed at lower frequencies and longer wavelengths (0.25 Hz maximum frequency and \sim 25 km wavelength). Positive pulses at 5–5.5 s can be traced from site BKWL through to site HAWL, whereas the eastern (shallower) feature is clear beneath sites L61B, QUA2 and K62A. Beneath site

Figure 2. Receiver function (RF) analysis results for stations SHLB (panels a–d) and L61B (panels e–h). (a and e) Map of earthquakes (green circles) used in the analysis. (b and f) Single-station stacked (over all backazimuths) Q component RF. Green line marks the inferred Moho pulse, and gray line marks zero time. (c and g) Backazimuth sweep showing Q and T component RFs as a function of event backazimuth. Vertical lines are as in panels (b and f). (d and h) Harmonic decomposition results; each trace corresponds to a particular term in the decomposition, as indicated at right. Vertical lines are as in panels (b and f). The harmonic decomposition method applied to this station illustrates a challenge of the method; there is energy in several of the higher-order terms, which complicates the differentiation between dipping and anisotropic features.

ons) on Wiley Online Library for rules of use; OA articles are governed by the applicable Creative Commons Licenso

15252027, 2024, 10, Downloaded from https://agupubs.onlinelibrary.wiley.com/doi/10.1029/2024GC011570 by Yale University, Wiley Online Library on [23/10/2024]. See the Terms

Figure 4. Profile section showing stacked Q-component RFs, computed at frequencies up to 0.5 Hz, plotted at the longitudes of the corresponding seismic stations (names at top). Topography is plotted in the upper panel. See Figure 1 for site locations in map view.

SHLB, the character of the RF traces appear to be strongly frequency dependent; they show weak pulses at different times in the higher and lower frequency analysis.

To summarize, from our examination of RFs at different frequencies and our analysis of the relative amplitude of the observed pulses (Figure 5), the shallow pulse at 3.5 s observed in the eastern stations of the array (sites L61B, QUA2, K62A) and the deep pulse at 5–5.5 s observed in the western stations (sites BKWL, K61A, WILL, NPND) are visible in all frequency bands (0.25 Hz, 0.5 Hz, 1 Hz). Thus, we can infer abrupt changes in impedance across a small depth range at these boundaries. At low frequencies, the deeper pulse is not visible at sites SHLB and L61B, and the shallower pulse is not visible at sites HAWL and NPND.

4.3. Directional Dependence of RF Pulses

Near-horizontal, laterally homogenous boundaries in isotropic seismic properties should produce Ps converted waves that do not change as a function of direction (e.g., Cassidy, 1992; Levin & Park, 1998). To test whether this is the case for our data, we created a comparison of RF traces from WILL and HAWL for three different backazimuthal swaths (Figure 6). We plot the traces as a function of epicentral distance to allow us to rule out the possibility of interference from multiple reflections; the moveout of the pulses we interpret indicates that they are primary conversions and not multiple reflections (Figure 6). We also applied this method to all of our stations (Figures S9–S14 in Supporting Information S1). Station WILL is located near the west side of our array, above Laurentian crust, whereas HAWL is located at the center of our array configuration, above Moretown terrane crust, approximately 10 km east of the suture with Laurentia. We compare these stations to demonstrate the variability in the directional dependence of RF behavior between stations. WILL and HAWL were chosen as representative stations from the western and central portions of the array, respectively; neighboring stations of each show similar behavior. Q-component RF traces from WILL and HAWL are arranged in backazimuth quadrants $90^{\circ}-180^{\circ}$, $180^{\circ}-270^{\circ}$, and $270^{\circ}-360^{\circ}$ (Figure 6). There are very few events in the data set from the $0^{\circ}-180^{\circ}$ 90° quadrant due to a lack of sources to the northeast of our array; thus, we do not show them. The details of where we decide to draw the quadrant boundaries do not change our interpretations, as shown in Figure S15 in Supporting Information S1.

WILL shows a constant change in impedance from all backazimuth directions at ~ 5.5 s, with some minor variations between quadrants; this is generally consistent with a (nearly) horizontal boundary at depth (Figure 6a). The Ps arrival time is nearly constant for all epicentral distances, which is an expected outcome given the moveout correction applied during data processing. This pulse is overprinted by possible multiple reflections from an intracrustal feature in the quadrants $90^{\circ}-180^{\circ}$ and $270^{\circ}-360^{\circ}$. In contrast, the RF traces from HAWL show significant

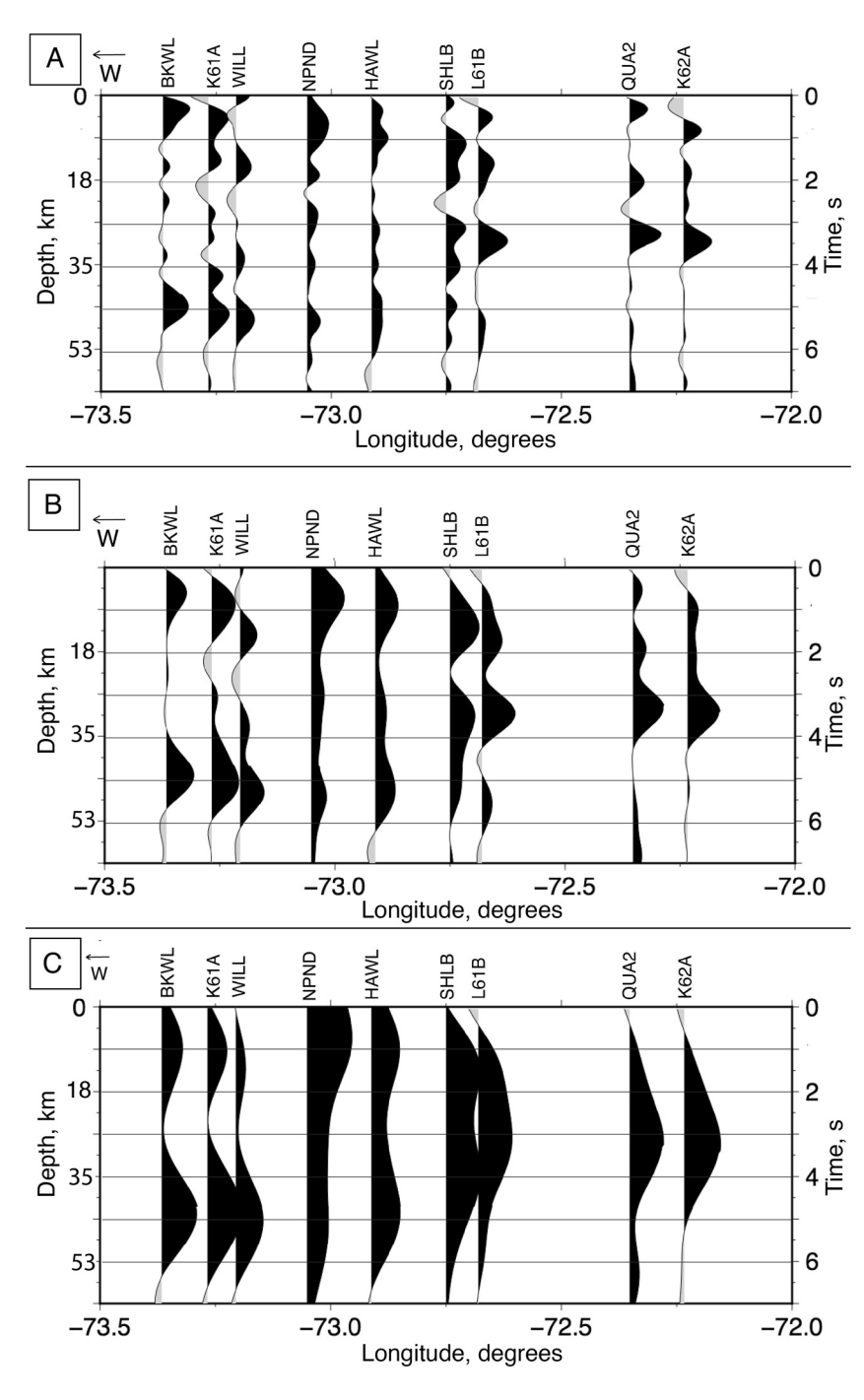


Figure 5. (a) Single-station stacked Q component receiver function transect, calculated using a 1 Hz cutoff frequency. (b) Same as panel (a) but calculated using a 0.5 cutoff frequency, as shown in Figure 3c. Same as panel (a) but calculated using a 0.25 cutoff frequency.

directional dependance (Figure 6b). We can identify a positive pulse at approximately 5.5 s, similar to the one seen in data from site WILL. However, it is not a constant feature across all directions. It is clearly observed in data for quadrants $180^{\circ}-270^{\circ}$ and $270^{\circ}-360^{\circ}$, where it shows a clear difference in arrival time as a function of source distance (black dashed line). This pulse is weak or missing in the data for quadrant $90^{\circ}-180^{\circ}$.

We also made an additional comparison between the results of directional analysis of RFs from stations WILL and HAWL, including source distributions (Figure 7a), backazimuthal Q component RF gathers (Figure 7b), single-

1525/2027, 2024, 10, Downloaded from https://agupubs.onlinelbrary.wiley.com/doi/10.1029/2024GC01157/0by Yale University, Wiley Online Library on [23/10/2024]. See the Terms and Conditions (https://onlinelibrary.wiley.com/terms-and-conditions) on Wiley Online Library for rules of use; OA artic

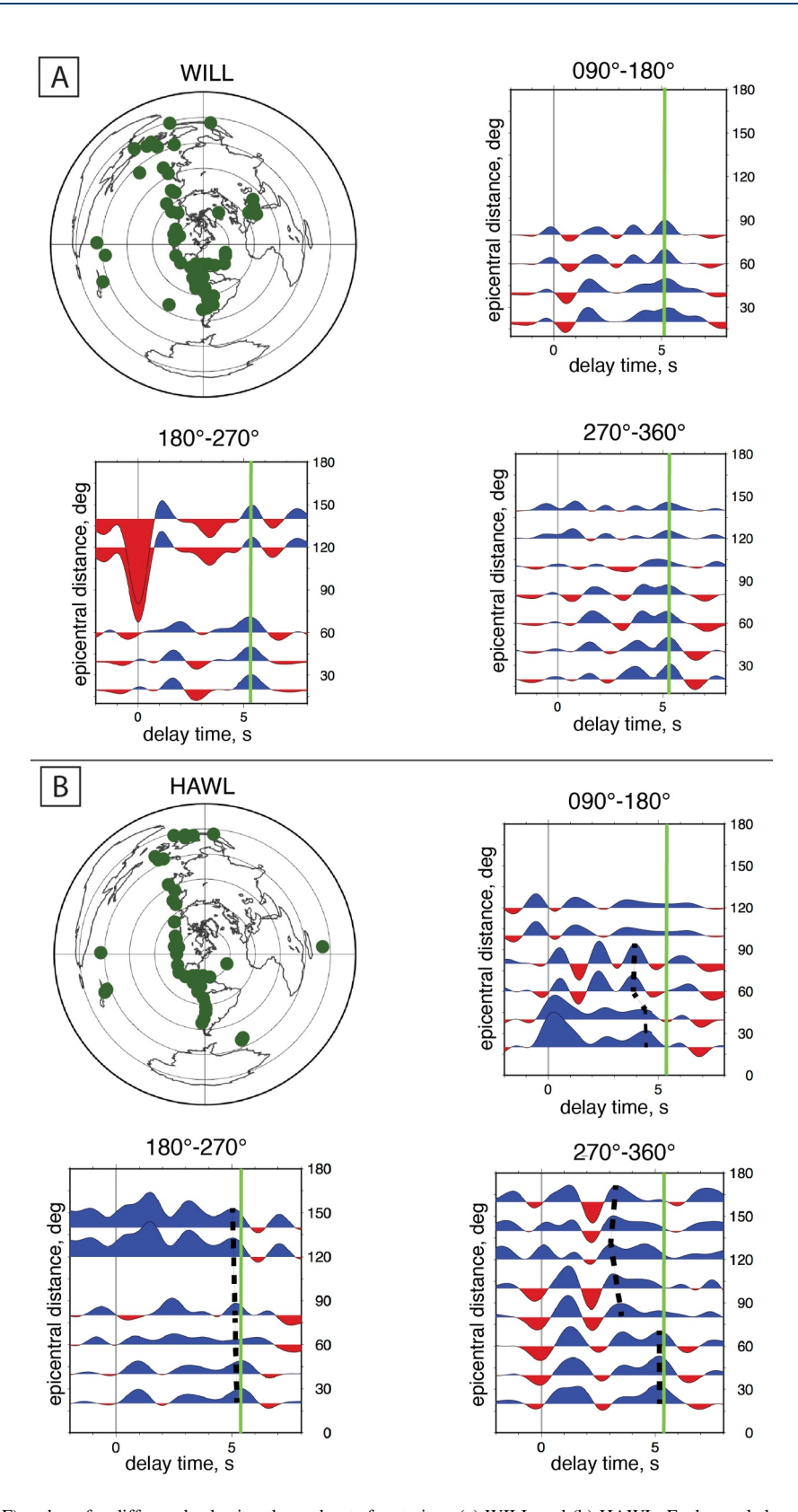


Figure 6. Receiver function (RF) gathers for different backazimuth quadrants for stations (a) WILL and (b) HAWL. Each panel shows a map of earthquake sources (upper left) and *Q*-component RF gathers from three different backazimuth ranges (labels at top; upper right and bottom panels) presented as a function of epicentral distance. Green lines represent the expected Moho arrival based on the single-station *Q* component stacks; black dashed lines represent observed *P*s arrivals showing directional dependence.

1525/207, 2024, 1, D. Downloaded from https://agupubs.o.inielbrary.wiel.com/doi/10.1029/2024GC011570 by Yale University, Wiley Online Library on [23/10/2024]. See the Terms and Conditions (https://onlinelibrary.wiley.com/terms-and-conditions) on Wiley Online Library for rules of use; OA articles are governed by the applicable Creative Commons Licensia

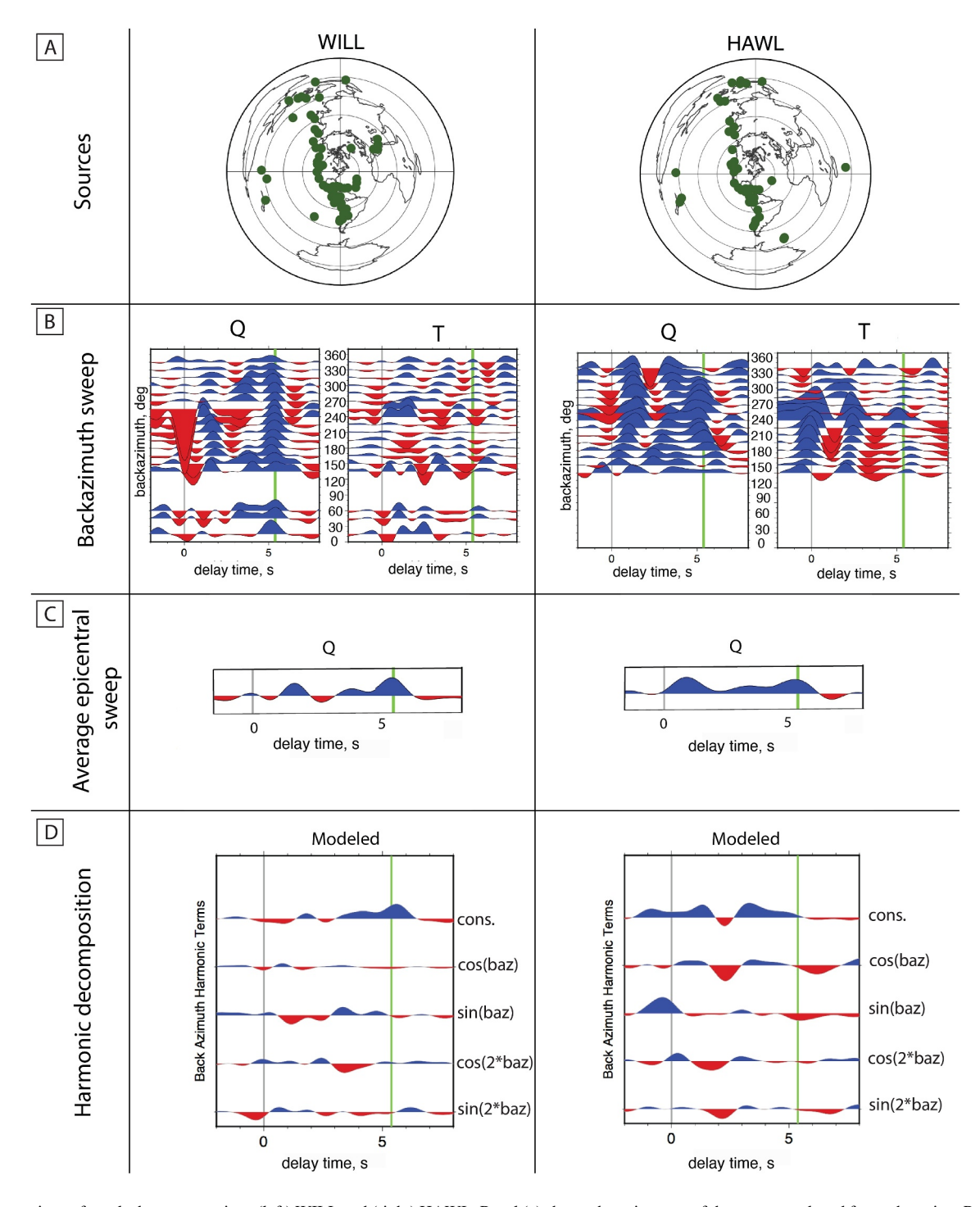


Figure 7. Comparison of results between stations (left) WILL and (right) HAWL. Panel (a) shows the epicenters of the events analyzed for each station. Panel (b) shows backazimuthal gathers of (left) Q and (right) T component RFs. Station WILL has a constant pulse at 5.5 s for component Q and no conspicuous arrival at 5.5 s on the T component. In contrast, station HAWL does not show a consistent Ps arrival time on the Q component; rather, the pulse arrival time is dependent on the direction. HAWL does show an arrival on the T component at \sim 5 s and 240°. Panel (c) shows stacked Q component RFs; both stations show a pulse at \sim 5 s. Panel (d) shows the harmonic decomposition results (modeled components only). Station WILL has a significant Moho pulse only on the constant component (cons). HAWL shows a negative pulse on the sin(baz) component at \sim 5.5 s, a negative pulse on the cos(baz) and sin(baz) components at \sim 6 s, and a positive pulse on the constant component at \sim 3.5 s.

station stacked RFs (Figure 7c), and harmonic decomposition results (Figure 7d). At site WILL, we observe a pulse at the same time (\sim 5 s) from every direction, visible in the backazimuth gather (Figure 7b), the stack of all Q-component data (Figure 7c), and the constant component in the harmonic decomposition (Figure 7d). In

contrast, at site HAWL, a clear pulse appears in the backazimuth gather on component Q at times 4.5–6 s, with its timing depending on direction (Figure 7b). Furthermore, the arrivals on component T are not constant across directions. The intra-crustal pulses show features that produce flipped polarities and time difference in arrivals, and the Moho pulse can only be clearly identified at backazimuths near \sim 240°. We also observe that for station HAWL, this Ps pulse has an arrival time (\sim 5 s on the Q-component stack backazimuth sweep; Figure 7c) that does not match with the arrival of the constant component of the harmonic decomposition plot (Figure 7d). Instead, an earlier (\sim 3.5 s) pulse is clear on the constant component. The second-order positive pulses at \sim 6 s on the Q stacked components and the harmonic decomposition terms might reflect multiply reflected waves; therefore, we do not interpret them as primary conversions. Station HAWL exhibits a clear mismatch between the single-station Q-component stack and the constant harmonic component trace, which likely points to lateral heterogeneity in the structure beneath the NEST line. Specifically, lateral heterogeneity at depth limits the effectiveness of the harmonic decomposition method as it assumes lateral homogeneity beneath the station.

We also examined neighboring stations to understand whether they exhibit similar behavior. Stations SHLB and L61B show less significant mismatches between the expression of the Moho converted pulse on the single-station Q-component stacks and the harmonic decompositions (Figure 2). The backazimuth sweep from station L61B (Figure 2f) shows a positive pulse at \sim 4 s on the Q component. The constant component of harmonic expansion exhibits a weak pulse at the same time, whereas the T component pulse systematically varies in polarities and amplitudes. A weak negative pulse at ~4 s is visible as energy on the cos(baz) and sin(baz) components (Figure 2h). We also see evidence for complex intra-crustal layering on both components at this station. At station SHLB, the stack of Q components and the constant component of the harmonic decomposition both show a positive pulse between 3 and 4 s (Figures 2c and 2d). For the T component, there is a strong directionally variable pulse present immediately before the 5 s pulse (Figure 2c), with a corresponding pulse on the sin(baz) harmonic decomposition term (Figure 2d). We also investigated directional dependence at other stations for which the data coverage was sufficient to make this analysis (see Figures S9 in Supporting Information S1: BKWL, S10: K61A, S11: K62A, S13: QUA2). Station NPND did not have sufficient backazimuthal coverage. Stations K61A, K62A, QUA2, and WILL show reasonable consistency between the single-station Q component and the constant component from the harmonic decomposition. We therefore use Q-component stacks to develop a model of the Moho structure beneath this region, incorporating both stations with no directional dependence variability and those that do show directional dependence.

5. Discussion

5.1. Crustal Thickness Transition and Moho Structure

The closely spaced stations (10-15 km) in our array across the abrupt crustal change in depth to Moho make it possible to resolve the transition between Laurentia and the Moretown terrane in detail. C. Li et al. (2018) used seismic stations separated by ~70 km to describe the Moho step beneath our study region as a (nearly) vertical boundary in the crust between Laurentia and Gondwanan-derived terranes. C. Li et al. (2018) showed that Ps arrivals beneath the Grenville belt of Laurentia have delay times ranging from 4.5 to 6 s, whereas stations on the Gondwanan-derived terranes (Moretown and Ganderia) have delay times ranging from 3 s (Moretown and Ganderia) to 4 s (Avalonia). The corresponding Moho depth estimates vary from 40 to 55 km for Grenville crust and from 25 to 35 km beneath Gondwanan-derived terranes (Figure 1b). Our determination of Ps delay times for sites K61A, K62A, L61B and QUA2 are within 0.1 s of those reported by C. Li et al. (2018). Our results show that the dramatic change in Ps arrival times from 5.2 to 3.5 s, representing a crustal thickness change from approximately 46-31 km, respectively, occurs between sites HAWL and SHLB (Figure 8) over a distance of less than 15 km. Crucially, several stations in the center of the array appear to record both the smaller and larger Ps arrival times in the single-station stacks (Figure 8). Stations NPND, HAWL, SHLB, and L61B show two pulses, one at \sim 3.5 s and another at \sim 5.5 s; our interpretation of the complex traces beneath these stations is that they reflect the presence of a dipping layer and/or a layer with anisotropic properties that creates direction-dependent P-SV and P-SH conversions at ~48 km depth. The earthquake backazimuthal coverage for station NPND is poor compared to stations HAWL, SHLB, and L61B. Despite this, the RF patterns are very similar, leading us to interpret them collectively. Furthermore, given that station L61B and the stations to its west (SHLB, HAWL and NPND) show a complex series of interfering pulses that are difficult to interpret, we hypothesize that L61B represents the eastern edge of a complex, highly deformed volume of lower crust near the terrane boundary (Figure 8). The configuration of our array does not allow us to trace this complex zone east of station L61B. However, station QUA2 does

15252027, 2024, 10, Downloaded from https://agupubs.onlinelibrary.wiley.com/doi/10.1029/2024GC011570 by Yale University, Wiley Online Library on [23/10/2024]. See the Terms and Condition

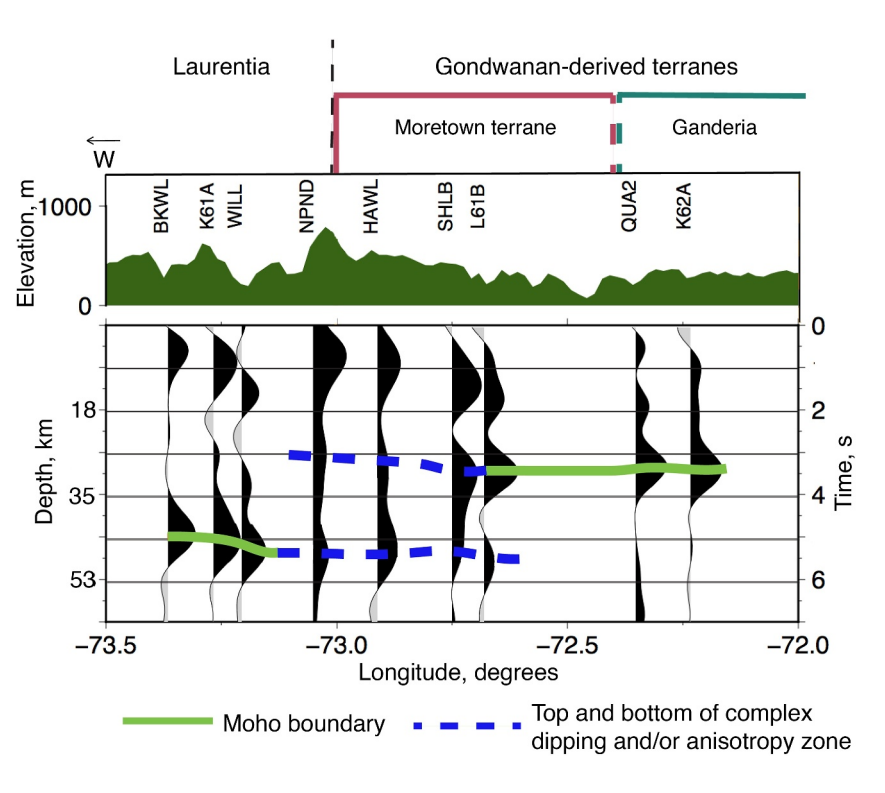


Figure 8. Lithospheric structure reflected by stacked Q component RFs for all stations compared to tectonic boundaries, shown at the top. Receiver function stacks are plotted at the location of the corresponding station along the New England Seismic Transects line. Solid green line represents the location of the Moho based on clear pulses, whereas dashed blue line represents the boundaries of the complex zone associated with dipping and/or anisotropic layers based on the harmonic decomposition analysis. Note that the boundary between the Moretown terrane and Ganderia is approximate.

not show evidence for a dipping and/or anisotropic layer; therefore, we can infer that the complex region near the Laurentia-Moretown terrane suture zone crust transitions to a simpler crust between L61B and QUA2, which are \sim 25 km apart (Figure 8).

The Moho boundaries identified with the RF stacks are corroborated by interpretations based on our *P*-to-*S* conversion points map (Figure 3). The geographic distribution of these conversion points, combined with our directional dependency analysis, is useful to further analyze the geometry of the Moho in specific geographic regions. For instance, stations K61A and WILL show piercing points that sample the Moho to the NW of these stations. In the backazimuth sweep plot, the Moho boundary to the NW of these sites is identified at a depth of ~44 km (Figures S3 and S7 in Supporting Information S1). Similarly, *P*-to-*S* conversion points that sample the Moho to the SE and NW, respectively, of sites L61B and QUA2 illuminate the geographic sampling of a Ps pulse at ~3.2 s incoming from the corresponding backazimuths (Figures S12 and S13 in Supporting Information S1).

If the pulses at ~ 3.5 s on the east of our array and ~ 5.5 s on the west of our array indeed represent the Moho, then one possible interpretation of our data involves a doubling of the Moho that suggests an overthrusting structure. This interpretation is strikingly similar to inferences based on observations made in northern Connecticut by Luo et al. (2021, 2022) at stations of the SEISConn line. These studies imaged the Moho structure 75 km to the south of our study area using both RF analysis (Luo et al., 2021) and scattered wave migration imaging (Luo et al., 2022) and observed overlapping Moho boundaries in a geometry that appears similar to what we observe beneath NEST. Similar to our work, the complex transitional region between thick and thin crust, beneath stations with particularly complex RF traces, lies beneath the Moretown terrane and the eastern edge of Laurentia. This in turn suggests that deformation linked with some combination of Moretown terrane accretion, post-accretion modification via metamorphism, and/or later reactivation of pre-existing Taconic structures by compression and shortening may have controlled the creation of the complex crustal structure (Luo et al., 2021, 2022). An alternative interpretation is that the complex zone located between stations NPND and L61B consists of anisotropic layers that are not delineated by Moho boundaries. The abrupt change in crustal thickness and the presence

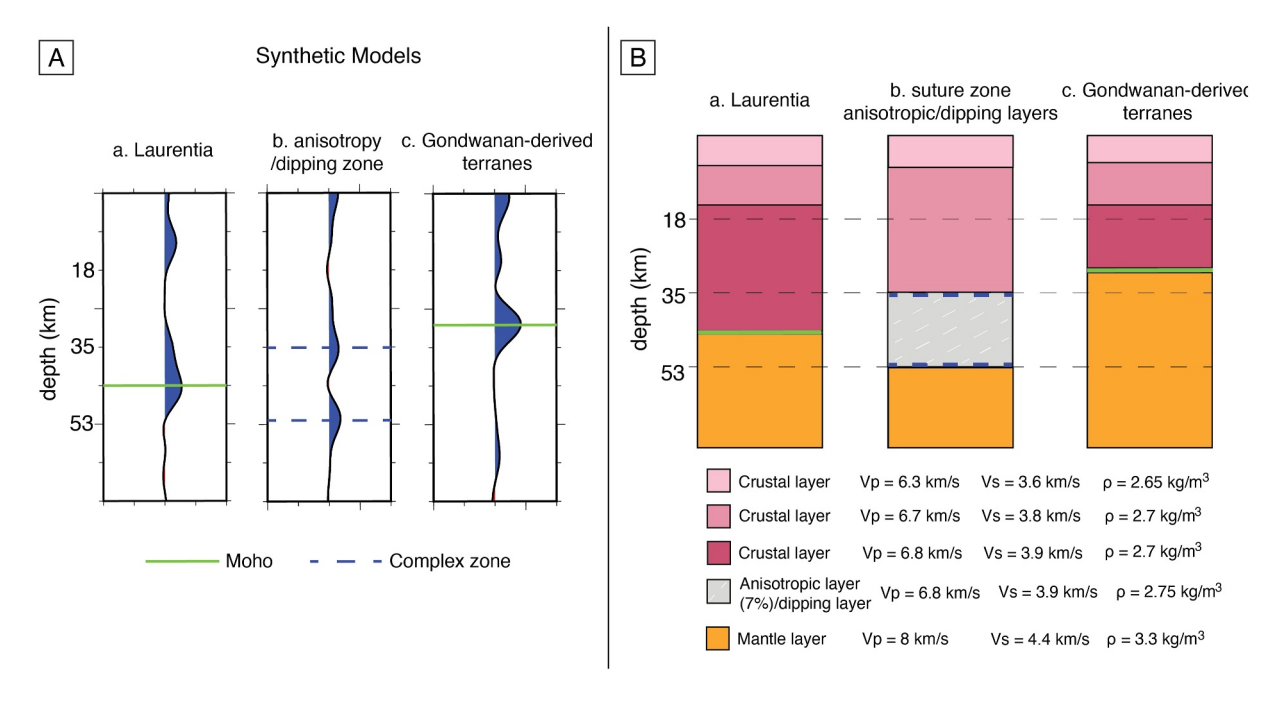


Figure 9. (a) Results of synthetic seismogram modeling for the three sections of our transect using modeling parameters are illustrated in panel (b). (a) Modeled RFs for a model representing stations in the western end of our transect: BKWL, K61A and WILL, which are located above Laurentia. (b) Modeled RFs for a model representing stations in the middle of our transect: NPND, HAWL, SHLB, L61B, which are on top of the transition between Laurentian and accreted terrane crust, where anisotropic and/or dipping interfaces were identified. (c) Modeled RFs for a model representing stations in the eastern end of our transect: QUA2, K62A, which are on top of Gondwanan-derived accreted terranes. (b) Schematic diagrams of model parameters used to generate the synthetic RFs are shown in panel (a). We indicate the *P*-wave and *S*-wave velocity, density, and anisotropy for each layer.

of a shear zone might result from post-orogenic deformation. This deformation might have caused the rocks between Laurentia and Moretown to accommodate and endure higher stress levels, and more strain, than the more distal end of the Moretown terrane; this deformation is reflected by the harmonic decomposition analysis results on stations above the shear zone.

In order to test the robustness of the RF features that we interpret, we show in Figure 9a a simple forward modeling experiment in which we generate synthetic seismograms using the parameters shown in Figure 9b (Chen et al., 2021) for a simplified model consistent with the tectonic interpretation shown in Figure 8. To simulate the crust of the Moretown terrane, we included an upper isotropic zone above an anisotropic zone, which is located at a depth range of 35–52 km, where we identified the complex zone from our data. This zone is characterized by higher V_p and V_s values. Additionally, we included another isotropic layer beneath the anisotropic zone, also exhibiting increased V_p and V_s values, to represent the mantle. The velocity increases at the interfaces between each layer. Our model explicitly seeks to replicate major features based on a plausible the configuration of the inferred eastward-dipping rifted Laurentian crust, as well as the complex zone near the abrupt change in crustal thickness and the Gondwanan-derived Moretown terrane. This forward modeling exercise, while not unique, shows that the major features of the RFs can be explained by our preferred interpretation.

5.2. Possible Models of Past Tectonic Events

If the seismically complex region indeed represents overlapping Moho boundaries beneath NPND, HAWL, SHLB, and L61B, it may shed light on the suture between Laurentia and the Moretown terrane and the nature of a possible transition zone between them. Hillenbrand et al. (2021) presented 40 Ar/ 39 Ar thermochronological evidence suggesting that the crust underlying accreted Gondwanan-derived terranes in southern and central New England formed a 50–60 km thick Acadian plateau during the time interval between 380 and 330 Ma. In this model, the suture between Laurentia and the Moretown terrane formed the western boundary of the plateau, with the presumably stronger Laurentian crust forming a buttress to allow compression and shortening to substantially thicken the crust beneath the accreted terranes. Hillenbrand et al. (2021) further suggested that beginning at 330 Ma, orogen-parallel ductile flow enabled plateau collapse. A combination of plateau collapse and erosion/



15252027, 2024, 10, Downloaded from https:/

library.wiley.com/doi/10.1029/2024GC011570 by Yale University, Wiley Online Library on [23/10/2024]. See the Terms

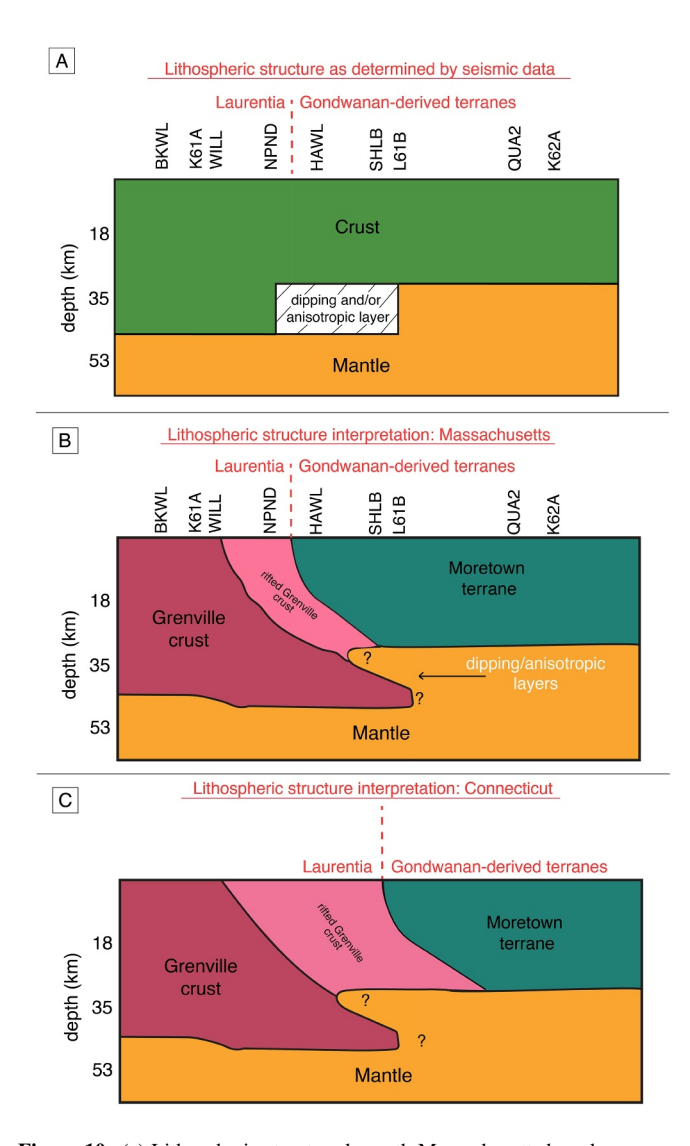


Figure 10. (a) Lithospheric structure beneath Massachusetts based on seismic data processed in this study. The seismic data effectively identify the crust, mantle and Moho boundary. However, it cannot distinguish between Laurentia and Gondwanan-derived terrane crusts. RFs and harmonic decomposition analysis distinguish between dipping and/or anisotropic layers and isotropic layers. (b) Interpretation of lithospheric structure beneath Massachusetts based on geophysical data at depth and geological data at the surface. The boundary between the Grenville belt of the rifted Laurentian margin and Moretown terrane was identified at the surface (Karabinos et al., 2017; Macdonald et al., 2014). This interpretation shows the Laurentian-Moretown suture dipping east from the surface boundary to the western end of the shallow Moho interface. A zone of rifted Grenville crust separating the Moretown terrane from unrifted Grenville crust also dips eastward. The complex anisotropic region between the prominent shallow and deep Moho interfaces, which extends from NPND eastward to L61B, may be composed of highly deformed rifted Grenville crust intercalated with oceanic crust and mantle rocks. (c) Interpretation of lithospheric structure beneath Connecticut based on Luo et al. (2023). This interpretation is similar to that in panel (a), but the suture between Laurentia and the Moretown terrane is east of the abrupt step in depth to Moho in Connecticut, whereas it is west of the step in Massachusetts.

isostatic adjustment led to the present-day crustal thickness of approximately 30 km, indicating a loss of 20–30 km of overlying material (Hillenbrand et al., 2021). One scenario is that the Grenville crust and the thickened Moretown crust were both roughly 50 km thick on either side of the suture zone when the Acadian plateau existed; subsequently, the thickness of the Moretown terrane crust decreased dramatically (by \geq 20 km) after plateau collapse, whereas the Grenville crustal thickness decreased less (\sim 5 km), resulting in a current offset in the Moho depth of approximately 15 km.

There is no reliable way to estimate the thickness of the Moretown terrane crust before its Taconic accretion along the Laurentian margin. Based on current thickness and denudation estimates (Hillenbrand et al., 2021), it seems reasonable to assume that the undeformed Grenville crust was approximately 50 km thick. However, the rifted Laurentian margin, composed of Grenville crust that had been modified and thinned by Neoproterozoic extension and normal faulting, must have been substantially thinner than 50 km when it was overridden by the Moretown terrane in the east-dipping subduction zone. Any cross-section through the Laurentian-Moretown suture zone immediately following Taconic accretion is conjectural; however, a plausible scenario is that the suture was a lithosphere-penetrating east-dipping structure that juxtaposed the Moretown terrane on rifted Grenville crust. The rifted Grenville crust likely formed a buffer zone between the Grenville crust that was undeformed or weakly deformed during Neoproterozoic rifting and Paleozoic tectonism and the accreted Moretown terrane.

A simplified sketch of the present-day lithospheric geometry based on geophysical data at depth is shown in Figure 10a. Alone, the geophysical data are inadequate to differentiate between the tectonic units; therefore, these interpretations integrate our seismic data with previous insights from geological investigations (e.g., Hillenbrand et al., 2021; Karabinos et al., 2017; Macdonald et al., 2014) and also incorporate inferences from previous studies elsewhere in New England (Luo et al., 2021, 2022). Our preferred interpretation, which represents a plausible (although not unique) model, is shown in Figure 10b. In this model, which invokes an overthrusted Moho near the Laurentia-Moretown suture, the suture dips east from the surface boundary to the western end of the shallow Moho converter. The eastdipping belt of the rifted Grenville crust separates the Moretown terrane from the unrifted Grenville crust, and it also dips eastward. The western boundary of the rifted Grenville crust at the surface corresponds to Grenville rocks in the Green Mountain and Berkshire massifs. At depth, it intersects the prominent, deeper western Moho converter. The complex anisotropic region between the prominent shallow and deep Moho interfaces, which extends from NPND westward to L61B, may be composed of highly deformed rifted Grenville crust intercalated with oceanic crust and mantle rocks due to crustal shortening and thrusting during and after the accretion of the Moretown terrane. Rocks in the paleo-subduction zone were certainly deformed during Taconic accretion of the Moretown terrane, and were probably deformed during the Acadian accretion of Avalonia and during the long interval of the Acadian plateau (380-330 Ma). Thus, the zone between NPND and L61B between 30 and 45 km depth may be both anisotropic and dipping, consistent with the higher-order terms observed on the harmonic decomposition traces at these stations.

The interpretation shown in Figure 10c for northwestern Connecticut is based on Luo et al. (2023), who analyzed data from the SEISConn experiment 75 km to the south of our study area, and is similar to that of Figure 10b for

northwestern Massachusetts. The primary difference between the two cross-sections is that the abrupt Moho step is located west of the surface trace of the Laurentian-Moretown suture in Connecticut, whereas it is east of the suture in Massachusetts. The origin of this difference at different latitudes is not yet well understood. One simple explanation is that westward transport of the Moretown terrane was greater in Massachusetts than it was to the south in Connecticut, either during the Taconic orogeny or during later Acadian deformation. While the interpretation shown in Figure 10b is not unique, it is consistent with the major features of our RF observations and incorporates insights from the dense SEISConn array to the south.

Our model and that proposed by Luo et al. (2023) for Connecticut share some features with models proposed for the southern New England Moho step by C. Li et al. (2018) and Hillenbrand et al. (2021), but also differ in some critical aspects. Specifically, both C. Li et al. (2018) and Hillenbrand et al. (2021) proposed a vertical or steep boundary between Laurentia and the Moretown terrane that coincided with the Moho step. In contrast, our imaging, based on the densely spaced NEST array, and that of Luo et al. (2021, 2022, 2023), based on the densely spaced SEISConn array, have both yielded evidence for a complex zone of dipping and/or anisotropic structure near the suture. Luo et al. (2021, 2022) interpreted their images as reflecting a zone of overlap between a shallower and deeper Moho with an overthrust-type geometry; our preferred model also invokes such a "doubled Moho" geometry. Specifically, we propose that the compression and shortening that formed the Acadian plateau in the model of Hillenbrand et al. (2021) was responsible for reactivating east-dipping faults and producing the lithospheric-scale overthrust structure inferred beneath southern New England.

Although C. Li et al. (2018) interpreted the decrease in depth to Moho from Grenville to the accreted Appalachian crust as an abrupt change in southern New England, they suggested a much smoother transition—i.e., with a similar decrease in depth occurring over a greater horizontal distance—in northern New England. This suggests that post-accretion events that affected the suture after the arrival of the Moretown terrane played an important role in creating the sharp Moho step in southern New England inferred from our data in northwestern Massachusetts and reported by Luo et al. (2021, 2022) to the south in Connecticut. Interestingly, the abrupt Moho step we image in this study, and that Luo et al. (2021, 2022) imaged beneath Connecticut, is not present elsewhere along the Appalachian margin, either to the north (C. Li et al., 2018) in northern New England or to the south (Luo et al., 2023) in the central or southern Appalachians. The similarity between our results and those of Luo et al. (2021, 2022, 2023) suggest that the abrupt Moho step and overlapping shallow and deep Moho boundaries near the suture between Laurentian and accreted Appalachian terranes crust is a robust feature of southern New England and is closely tied to a combination of tectonic processes that was unique to this region, likely including the formation and collapse of the Acadian plateau (Hillenbrand et al., 2021). Our imaging results, in combination with the results of Luo et al. (2021, 2022, 2023), open a host of new questions regarding the tectonic evolution of southern New England. These include how the present-day Moho configuration has survived over hundreds of millions of years, how the rheology of the deep crust has affected its evolution, and what petrological and geodynamic processes have shaped the crustal architecture during various phases of Appalachian orogenesis.

6. Conclusions

We processed and analyzed seismic records from 1,048 earthquakes registered by nine stations located above the suture between Laurentia and the Moretown terrane suture, which was previously hypothesized to coincide with a \sim 15 km vertical step in the crust (C. Li et al., 2018). Using *P*-to-*S* RF analysis, in combination with a harmonic decomposition modeling technique, we obtained more detailed constraints on the nature of this boundary, taking advantage of a dense seismic station array.

We identified crust-mantle boundaries at two distinct depths; the deeper Moho is on the western side of the transect, between stations BKWL and WILL (Figures 1 and 4), at ~48 km depth with a gentle eastward dip. The shallower Moho is on the eastern side of the transect and is nearly horizontal beneath sites L61B to K62A at ~31 km depth (Figures 1 and 4). The abrupt change in depth to Moho occurs near the suture between Laurentia and the Moretown terrane over a lateral extent of less than ~30 km. In the central portion of the transect, between sites NPND and L61B, we identified interfaces delineating the top and bottom of a complex, likely anisotropic region. Our preferred interpretation is that these interfaces correspond to shallow and deep Moho boundaries, such that the zone of overlap exhibits a doubled Moho. The zone between the interfaces is likely composed of anisotropic crust and/or mantle material, as inferred by our harmonic decomposition analysis. The extension of this complex zone is constrained by data from stations NPND and L61B and it corresponds spatially to the suture between Laurentia



and the Moretown terrane. The anisotropic zone was almost certainly deformed during the Taconic accretion of the Moretown terrane, and was likely deformed again during the Acadian accretion of Avalonia.

Our preferred interpretation of the Moho geometry is similar to that documented by Luo et al. (2021, 2022, 2023) to the south beneath northwestern Connecticut. However, it is dissimilar to the more gradual change in crustal thickness observed across the Laurentian-Appalachian suture to the north (C. Li et al., 2018) and south (Luo et al., 2023) of our study region, suggesting differences in the tectonic processes that operated at different latitudes. The sharp lateral change in depth to Moho is spatially correlated with the narrow width of the Taconic and Acadian orogens in southern New England, and with the thickest crust in the Acadian plateau proposed by Hillenbrand et al. (2021). This spatial correlation suggests that the steep gradient in depth to Moho was caused by compression and crustal shortening during the Acadian accretion of Avalon and the existence of the Acadian plateau (Hillenbrand et al., 2021). In combination with previous studies, our results indicate that the change in crustal thickness is a robust feature of the suture between Laurentia and Gondwanan-derived terranes in southern New England. If future studies using dense seismic arrays confirm that the gradient in crustal thickness across the suture is more gradual in northern New England (C. Li et al., 2018), where the Acadian plateau was not as thick (Hillenbrand et al., 2021), it will support the hypothesis that crustal shortening during the formation of the Acadian plateau modified the Taconic suture between Laurentia and the Moretown terrane, thereby setting the stage for the evolution of the crust to its present-day architecture following plateau collapse.

Data Availability Statement

The Generic Mapping Tools (Wessel et al., 2013) were used to generate figures. The Receiver Function timeseries (RF) analysis was processed with the Recfunk21 code package (https://zenodo.org/records/12797942). The data used are available through the IRIS Data Management Center (https://ds.iris.edu/mda/7O/). Data from the NEST experiment is archived at the DMC (https://doi.org/10.7914/SN/7O_2018) and will be publicly available in 2025. We also used data from the USArray Transportable Array (https://ds.iris.edu/mda/TA/) and the New England Seismic Network (https://ds.iris.edu/mda/NE/) in this study.

References

Ammon, C. J. (1991). The isolation of receiver effects from teleseismic *P* waveforms. *Bulletin of the Seismological Society of America*, 81(6), 2504–2510. https://doi.org/10.1785/bssa0810062504

Ando, C. J., Czuchra, B. L., Klemperer, S. L., Brown, L. D., Cheadle, M. J., Cook, F. A., et al. (1984). Crustal profile of a mountain belt: COCORP deep seismic reflection profile in New England and implications for architecture of convergent mountain chains. AAPG Bulletin, 68, 819–837.
 Bianchi, I., Park, J., Agostinetti, N. P., & Levin, V. (2010). Mapping seismic anisotropy using harmonic decomposition of receiver functions: An application to Northern Apennines, Italy. Journal of Geophysical Research, 115(B12), B12317. https://doi.org/10.1029/2009jb007061

Bostock, M. G. (1998). Mantle stratigraphy and the evolution of the Slave province. *Journal of Geophysical Research*, 103(B9), 21183–21200. https://doi.org/10.1029/98jb01069

Bourke, J., Levin, V., Linkimer, L., & Arroyo, I. (2020). A recent tear in subducting plate explains seismicity and upper mantle structure of southern Costa Rica. *Geochemistry, Geophysics, Geosystems*, 21(12), e2020GC009384. https://doi.org/10.1029/2020GC009300

Bourke, J., Link, F., Li, Y., Masis, R., Espinal, K., Luo, Y., et al. (2023). Sharpness estimates of the New England crust-mantle transition, Abstract (1396065). In *Paper presented at AGU 2023, 11–15 December*.

Bourke, J., Vadim, L., Arroyo, I., & Linkimer, L. (2023). Evidence for Caribbean plate subduction in southern Costa Rica. *Geology*, 51(4), 408–412. https://doi.org/10.1130/g50796.1

Bradley, D. C., Tucker, R. D., Lux, D. R., Harris, A. G., & McGregor, D. C. (2000). Migration of the Acadian orogen and foreland basin across the northern Appalachians of Maine and adjacent areas. U.S. Geological Survey Professional, 1624, 55. https://doi.org/10.3133/pp1624

Brown, L., Ando, C., Klemperer, S., Oliver, J., Kaufman, S., Czuchra, B., et al. (1983). Adirondack-Appalachian crustal structure: The COCORP northeast traverse. *Geological Society of America Bulletin*, 94(10), 1173–1184. https://doi.org/10.1130/0016-7606(1983)94<1173:acstcn>2.0.

Cassidy, J. F. (1992). Numerical experiments in broadband receiver function analysis. Bulletin of the Seismological Society of America, 81(6), 2504–2510. https://doi.org/10.1785/bssa0810062504

Chen, X., Park, J., & Levin, V. (2021). Anisotropic layering and seismic body waves: Deformation gradients, initial S-polarizations, and converted-wave birefringence. *Pure and Applied Geophysics*, 178(6), 2001–2023. https://doi.org/10.1007/s00024-021-02755-6

Gurrola, H., & Minster, J. (1998). Thickness estimates of the upper-mantle transition zone from bootstrapped velocity spectrum stacks of receiver functions. *Geophysical Journal International*, 133(1), 31–43. https://doi.org/10.1046/j.1365-246X.1998.1331470.x

Hatcher, R. D. (2010). The Appalachian orogen: A brief summary, from Rodinia to Pangea: The lithotectonic record of the Appalachian region. Geological Society of America Memoir, 206, 1–19. https://doi.org/10.1130/2010.1206(01)

Hildebrand, R. S., & Whalen, J. B. (2020). Arc and slab failure magmatism of the Taconic orogeny, western New England, USA. Geological Society, London, Special Publications, 503(1), 409–422. https://doi.org/10.1144/sp503-2019-247

Hillenbrand, I., Williams, M., & Jercinovic, M. (2022). Petrochronologic constraints on Paleozoic tectonics in southern New England. In S. J., Whitmeyer, M. L. Williams, D. A. Kellett, & B. Tikoff Laurentia: Turning points in the evolution of a continent, Geological Society of America Memoir 220 (pp. 1–28). https://doi.org/10.1130/2022.1220(25)

Hillenbrand, I., Williams, M., Li, C., & Gao, H. (2021). Rise and fall of the Acadian altiplano: Evidence for a Paleozoic orogenic plateau in New England. Earth and Planetary Science Letters, 560, 116797. https://doi.org/10.1016/j.epsl.2021.116797



Acknowledgments

The NEST seismic experiment was

supported by Yale University, Rutgers

Foundation under Grants EAR-2147536

(Yale), EAR-2146804 (Williams), and

EAR-2147426 (Rutgers). We are grateful

to the IRIS PASSCAL Instrument Center

at New Mexico Tech for their support of

the NEST deployment. The facilities of the

IRIS Consortium are supported by the

Advancement of Geoscience (SAGE)

Agreement EAR-1851048. We thank

participants in the NEST, SEISConn, and

GENESIS projects for useful discussions

about the New England Appalachians. We

anonymous reviewer helped us to sharpen

our interpretations and greatly improve the

Award under Cooperative Support

National Science Foundation's

Seismological Facilities for the

also thank Vadim Levin for his contributions to this research. Constructive

comments from Cong Li and an

presentation of the material.

University, and the National Science

- Hopper, E., Fischer, K. M., Rondenay, S., Hawman, R. B., & Wagner, L. S. (2016). Imaging crustal structure beneath the southern Appalachians with wavefield migration. *Geophysical Research Letters*, 43(23), 12054–12062. https://doi.org/10.1002/2016gl071005
- Hughes, S., & Luetgert, J. (1991). Crustal structure of the western New England Appalachians and the Adirondack Mountains. *Journal of Geophysical Research*, 96(B10), 16471–16494. https://doi.org/10.1029/91jb01657
- IRIS Transportable Array. (2003). USArray Transportable Array. International Federation of Digital Seismograph Networks, Other/Seismic Network. https://doi.org/10.7914/SN/TA
- Karabinos, P., Macdonald, F., & Crowley, J. (2017). Bridging the gap between the foreland and hinterland I: Geochronology and plate tectonic geometry of Ordovician magmatism and terrane accretion on the Laurentian margin of New England. American Journal of Science, 137(5), 515–554. https://doi.org/10.2475/05.2017.01
- Kennett, B. L., & Engdahl, E. R. (1991). Travel times for global earthquake location and phase association. *Geophysical Journal International*, 105(2), 429–465. https://doi.org/10.1111/j.1365-246x.1991.tb06724.x
- Langston, C. A. (1979). Structure under Mount Rainier, Washington, inferred from teleseismic body waves. *Journal of Geophysical Research*, 84(B9), 4749–4762. https://doi.org/10.1029/jb084ib09p04749
- Levin, V., Lebedev, S., Fullea, J., Li, Y., & Chen, X. (2023). Defining continental lithosphere as a layer with abundant frozen-in structures that scatter seismic waves. *Journal of Geophysical Research: Solid Earth*, 128(7), e2022JB026309. https://doi.org/10.1029/2022JB026309
- Levin, V., & Park, J. (1997). P-SH conversions in a flat-layered medium with anisotropy of arbitrary orientation. Geophysical Journal International, 131(2), 253–266. https://doi.org/10.1111/j.1365-246x.1997.tb01220.x
- Levin, V., & Park, J. (1998). P-SH conversions in layered media with hexagonally symmetric anisotropy: A cookbook. PAGEOPH, 151, 669–697. https://doi.org/10.1007/978-3-0348-8777-9 25
- Levin, V., VanTongeren, J. A., & Servali, A. (2016). How sharp is the sharp Archean Moho? Example from eastern Superior Province. Geophysical Research Letters, 43(5), 1928–1933. https://doi.org/10.1002/2016gl067729
- Li, C., Gao, H., & Williams, M. (2020). Seismic characteristics of the eastern North American crust with Ps converted waves: Terrane accretion and modification of continental crust. *Journal of Geophysical Research: Solid Earth*, 48(5), 368–373. https://doi.org/10.1130/G47022.1
- Li, C., Gao, H., Williams, M. L., & Levin, V. (2018). Crustal thickness variation in the northern Appalachian Mountains: Implications for the geometry of 3-D tectonic boundaries within the crust. Geophysical Research Letters, 45(12), 6061–6070. https://doi.org/10.1029/ 2018GL078777
- Li, Y., Levin, V., Nikulin, A., & Chen, X. (2021). Systematic mapping of upper mantle seismic discontinuities beneath northeastern North America. Geochemistry, Geophysics, Geosystems, 22(7), e2021GC009710. https://doi.org/10.1029/2021GC009710
- Long, M., & Levin, V. (2018). New England seismic transect [Dataset]. International Federation of Digital Seismograph Networks. https://doi.org/10.7914/SN/7O 2018
- Long, M. D., & Aragon, J. C. (2020). Probing the structure of the crust and mantle lithosphere beneath the southern New England Appalachians via the SEISConn deployment. Seismological Research Letters, 91(5), 2976–2986. https://doi.org/10.1785/0220200163
- Luo, Y., Long, M. D., Karabinos, P., Kuiper, Y. D., Rondenay, S., Aragon, J. C., et al. (2021). High-resolution Ps receiver function imaging of the crust and mantle lithosphere beneath southern New England and tectonic implications. *Journal of Geophysical Research: Solid Earth*, 126(7), e2021JB022170. https://doi.org/10.1029/2021JB022170
- Luo, Y., Long, M. D., Karabinos, P., Rondenay, S., & Masis Arce, R. (2023). First-order transition in Appalachian orogenic processes revealed by along-strike variation of the Moho geometry. *Journal of Geophysical Research: Solid Earth*, 128(12), e2023JB027024. https://doi.org/10.1029/ 2023JB027024
- Luo, Y., Long, M. D., Rondenay, S., Karabinos, P., & Kuiper, Y. D. (2022). Wavefield migration imaging of Moho geometry and upper mantle structure beneath southern New England. Geophysical Research Letters, 49(13), e2022GL099013. https://doi.org/10.1029/2022GL099013
- Macdonald, F. A., Ryan-Davis, J., Coish, R. A., & Karabinos, P. (2014). A newly identified Gondwanan terrane in the northern Appalachian Mountains: Implications for the Taconic orogeny and closure of the Iapetus Ocean. Geology, 42(6), 539–542. https://doi.org/10.1130/G35659.1
- Olugboji, T. M., & Park, J. (2016). Crustal anisotropy beneath Pacific Ocean islands from harmonic decomposition of receiver function. Geochemistry, Geophysics, Geosystems, 17(3), 810–832. https://doi.org/10.1002/2015gc006166
- Park, J., & Levin, V. (2000). Receiver functions from multiple-taper spectral correlation estimates. Bulletin of the Seismological Society of America, 90(6), 1507–1520. https://doi.org/10.1785/0119990211
- Park, J., & Levin, V. (2016). Statistics and frequency-domain moveout for multiple-taper receiver functions. *Geophysical Journal International*, 207(1), 512–527. https://doi.org/10.1093/gji/ggw291
- Savage, B., Covellone, B. M., & Shen, Y. (2017). Wave speed structure of the eastern North American margin. Earth and Planetary Science Letters, 459, 394–405. https://doi.org/10.1016/j.epsl.2016.11.028
- Schmandt, B., Lin, F. C., & Karlstrom, K. E. (2015). Distinct crustal isostasy trends east and west of the Rocky Mountain Front. *Geophysical Research Letters*, 42(23), 10290–10298. https://doi.org/10.1002/2015GL066593
- Schulte-Pelkum, V., & Mahan, K. H. (2014). A method for mapping crustal deformation and anisotropy with receiver functions and first results from USArray. Earth Planetarty Science Letters, 402, 221–233. https://doi.org/10.1016/j.epsl.2014.01.050
- Shen, W., & Ritzwoller, M. H. (2016). Crustal and uppermost mantle structure beneath the United States. *Journal of Geophysical Research: Solid Earth*, 121(6), 4306–4342. https://doi.org/10.1002/2016JB012887
- Storchak, D., Schweitzer, J., & Bormann, P. (2008). The IASPEI standard seismic phase list. Seismological Research Letters, 74(4), 761–772. https://doi.org/10.1785/gssrl.74.6.761
- Trabant, C., Hutko, A. R., Karstens, R., Ahern, T., & Aster, R. (2012). Data products at the IRIS DMC: Stepping stones for research and other applications. Seismological Research Letters, 83(5), 846–854. https://doi.org/10.1785/0220120032
- Valley, P. M., Walsh, G. J., Merschat, A. J., & McAleer, R. J. (2019). Geochronology of the Oliverian plutonic suite and the Ammonosuc volcanics in the Bronson Hill arc: Western New Hampshire, USA. Geosphere, 16(1), 229–257. https://doi.org/10.1130/GES02170.1
- van Staal, C. R., Whalen, J. B., Valverde-Vaquero, P., Zagorevski, A., & Rogers, N. (2009). Pre-Carboniferous, episodic accretion-related, orogenesis along the Laurentian margin of the northern Appalachians. Geological Society London Special Publications, 327(1), 271–316. https://doi.org/10.1144/SP327.13
- Waldron, J., McCausland, P., Barr, S., Schofield, D., Reusch, D., & Wu, L. (2022). Terrane history of the Iapetus Ocean as preserved in the northern Appalachians and western Caledonides. Earth-Science Reviews, 233, 104163. https://doi.org/10.1016/j.earscirev.2022.104163
- Wessel, P., Smith, W. H. F., Scharroo, R., Luis, J., & Wobbe, F. (2013). Generic mapping tools: Improved version released. Eos, Transactions American Geophysical Union, 94(45), 409–410. https://doi.org/10.1002/2013E0450001
- Zhu, L., & Kanamori, H. (2000). Moho depth variation in southern California from teleseismic receiver functions. *Journal of Geophysical Research*, 105(B2), 2969–2980. https://doi.org/10.1029/1999jb900322

